

## Photoneutron Cross Sections for $Zr^{90}$ , $Zr^{91}$ , $Zr^{92}$ , $Zr^{94}$ , and $Y^{89}$ †

B. L. BERMAN, J. T. CALDWELL, R. R. HARVEY,\* M. A. KELLY, R. L. BRAMBLETT, AND S. C. FULTZ  
*Lawrence Radiation Laboratory, University of California, Livermore, California*

(Received 10 May 1967)

Photoneutron cross sections, including  $\sigma[(\gamma,n) + (\gamma,pn)]$  and  $\sigma(\gamma,2n)$  for  $Zr^{90}$ ,  $Zr^{91}$ ,  $Zr^{92}$ ,  $Zr^{94}$ , and  $Y^{89}$ , and  $\sigma(\gamma,3n)$  for  $Zr^{94}$ , have been measured as a function of photon energy up to 30 MeV with a monoenergetic photon beam from positron annihilation in flight. The photon energy resolution varied from less than 300 keV at the lowest to 400 keV at the highest energies. The average neutron energy was determined simultaneously with the cross-section data. Nuclear information extracted from the data includes giant-resonance parameters, integrated cross sections, level densities, and threshold (and hence mass) values. In particular, it is found that a Lorentz-shaped curve gives an accurate representation of the total photoneutron cross section near the peak of the giant resonance, although in several cases there is important structure about 5 MeV above the giant resonance. The variation with neutron number and atomic weight of these quantities is studied for these nuclei near the  $N=50$  closed neutron shell.

### I. INTRODUCTION

THE study of the properties of nuclei near the closed neutron shell at  $N=50$  is a subject of widespread interest. From the point of view of photon-induced reactions, however, little previous work has been done in this mass region. To examine in detail the photon absorption process and its branching into various decay modes, a systematic study has been completed of the photoneutron processes in a series of five separated isotopes in the zirconium region of the periodic table. Two have  $N=50$  ( $Zr^{90}$  and  $Y^{89}$ ), and enable one to study the effect of varying the proton number. Here the residual nucleus is left by a  $(\gamma,n)$  reaction in either an even-odd or odd-odd configuration. The other three ( $Zr^{91}$ ,  $Zr^{92}$ , and  $Zr^{94}$ ) illustrate the effects of adding one, two, and four neutrons, respectively, to the closed neutron shell. In the case of the  $Zr^{91}(\gamma,n)Zr^{90}$  reaction, the residual nucleus is left in an even-even configuration.

The nuclear systematics studied with the present techniques include: (a) the parameters of the giant resonance, namely, the resonance energy, the peak cross section, and the width; (b) the integrated cross section and its moments; (c) the branching to the various decay modes, particularly the ratio of the  $(\gamma,2n)$  cross section to the total nuclear photon absorption cross section; (d) the goodness of fit of a Lorentz curve to the giant resonance; (e) the presence (or absence) of any structure above the giant-resonance region; and (f) the average energy of the photoneutrons.

Previous photoneutron measurements in the  $N=50$  region have been done with the use of bremsstrahlung as the source of photons, either by the activation technique on  $Zr^{90}$ , whereby the residual  $Zr^{89}$  nucleus can be left either in its ground state or in its 4.4-min isomeric state,<sup>1</sup> or by total-neutron-yield measurements, which have been carried out for a number of nuclei in this

region.<sup>2,3</sup> Both of these methods depend on a photon difference analysis of the data in order to arrive at cross sections, which sometimes has led to large discrepancies between comparable measurements in the past. In addition, the lack of neutron multiplicity measurements hampers the interpretation of both types of experiments. The only study of several nuclei in this mass region is that of Yergin and co-workers.<sup>2,3</sup> There have been no previous measurements reported for  $Zr^{94}$ .

### II. EXPERIMENTAL METHOD

Some details of the experimental method have been given elsewhere.<sup>4-9</sup> A summary of the general techniques is given here, together with some further details concerning those features which are pertinent to the present series of experiments.

The source of radiation used is the forward-going photon beam from the two-photon annihilation in flight of a beam of fast positrons. The positrons are created by pair production in a thick, high- $Z$  target located between the first and second sections of the Livermore electron linear accelerator. They then are accelerated in the second and third accelerator sections, energy-analyzed with a magnet-and-slit system, and allowed to impinge on a thin, low- $Z$  annihilation target, e.g., 0.030-in. Be. The positrons transmitted through the annihilation target are swept away with a magnet, while the photons strike the neutron-producing sample.

<sup>2</sup> R. Nathans and P. F. Yergin, *Phys. Rev.* **98**, 1296 (1955).

<sup>3</sup> P. F. Yergin and B. P. Fabricand, *Phys. Rev.* **104**, 1334 (1956).

<sup>4</sup> R. L. Bramblett, J. T. Caldwell, B. L. Berman, R. R. Harvey, and S. C. Fultz, *Phys. Rev.* **148**, 1198 (1966).

<sup>5</sup> S. C. Fultz, R. L. Bramblett, J. T. Caldwell, and N. A. Kerr, *Phys. Rev.* **127**, 1273 (1962).

<sup>6</sup> B. L. Berman, R. L. Bramblett, J. T. Caldwell, R. R. Harvey, and S. C. Fultz, *Phys. Rev. Letters* **15**, 727 (1965).

<sup>7</sup> J. T. Caldwell, R. L. Bramblett, B. L. Berman, R. R. Harvey, and S. C. Fultz, *Phys. Rev. Letters* **15**, 976 (1965).

<sup>8</sup> S. C. Fultz, J. T. Caldwell, B. L. Berman, R. L. Bramblett, and R. R. Harvey, *Phys. Rev.* **143**, 790 (1966).

<sup>9</sup> S. C. Fultz, J. T. Caldwell, B. L. Berman, R. L. Bramblett, M. A. Kelly, H. D. Wilson, M. S. Coops, R. W. Loughheed, J. E. Evans, and R. W. Hoff, *Phys. Rev.* **152**, 1046 (1966).

† Work performed under the auspices of the U. S. Atomic Energy Commission.

\* Now at University of Hawaii, Honolulu, Hawaii.

<sup>1</sup> P. Axel and J. D. Fox, *Phys. Rev.* **102**, 400 (1956).

The neutron counts produced by the positron bremsstrahlung are determined by repeating the measurements with electrons rather than positrons. The differences obtained give the net counts caused by the annihilation photons alone. Thus, a monoenergetic variable-energy photon source is obtained whose energy is equal to the kinetic energy of the positrons plus 0.76 MeV (deduced from the conservation of energy and momentum), and whose resolution is given by the combined contributions of the beam optics and the collision and multiple-scattering processes in the annihilation target. For the slit settings used, and for the 0.030-in.-thick Be target which was used in most of the present measurements, this resolution is about 2.0%, or 320 keV, in the giant-resonance region.<sup>4</sup> The absolute energy scale is known to within  $\frac{1}{4}$ %. Some data for Zr<sup>90</sup> (13 to 27 MeV) were repeated with a 0.010-in.-thick Be target, for which the photon energy resolution is about 1%.<sup>4</sup> The low-energy data (below 12.5 MeV) for Zr<sup>94</sup>, were taken with 4% resolution.

The collimated photon beam is monitored with a xenon-filled transmission ionization chamber located between the sweeping magnet and the sample. The response per annihilation photon of this ionization chamber is determined as a function of photon energy by use of a 5-in.-diam by 6-in.-thick NaI  $\gamma$ -ray spectrometer. A normalization between positron and electron runs is obtained under the assumption that the positron and electron bremsstrahlung spectra per particle are identical. Three methods, utilizing (a) the NaI spectrometer, (b) a Faraday cup, and (c) the neutron yield from deuterium, are used to determine this normalization. All of these methods yield the same results, but with the reproducibility sufficiently uncertain that there might be a systematic error as high as 4% in the normalization.

The sample specifications are given in Table I. The attenuation of the photon beam in the samples was taken into account and made necessary a correction to the data which varied from 10 to 20% for the separated zirconium isotopes and was 35 and 56% for the yttrium samples. The uncertainty in this correction is dependent upon the uncertainty in the atomic absorption coefficients, but a 3% uncertainty in this quantity results in only a 1% uncertainty in the yttrium cross sections, and in a negligible uncertainty for the other cases.

The neutron detector consists of a 2-ft cube of paraffin in which are inserted 48 high-pressure (167 cm Hg)BF<sub>3</sub> tubes arranged about a 3-in. axial hole in four concentric rings of 12 tubes each, at radial distances of 2.50, 4.25, 5.75, and 7.00 in., respectively, from the beam line. The sample is placed in the central beam hole. The signals from each ring are amplified and monitored separately. The number of neutrons detected for each beam burst is counted. The scalers are gated on shortly after each beam burst for a time

TABLE I. Sample specifications.

Nucleus	Mass (g)	Chemical form	Purity (%)	Principal impurity
Zr <sup>90</sup>	199.5	Metal	97.8	Other Zr isotopes
Zr <sup>90</sup>	67.6	Oxide	97.7	Other Zr isotopes
Zr <sup>91</sup>	53.8	Oxide	90.9	Zr <sup>90</sup> : 5.0%; Zr <sup>92</sup> : 3.3%
Zr <sup>92</sup>	55.5	Oxide	95.7	Zr <sup>90</sup> : 2.3%
Zr <sup>94</sup>	52.9	Oxide	96.5	Zr <sup>90</sup> : 1.9%
Y <sup>89</sup>	299.5	Metal	100.0	Negligible
Y <sup>89</sup>	458.0	Metal	100.0	Negligible
Natural Zr	211.5	Metal	100.0	Negligible

interval of 300  $\mu$ sec, which is several times longer than the decay time of the detector (about 90  $\mu$ sec) but short compared to the time between beam bursts when the accelerator is operated at its usual repetition rate of 360 pulses per second. The multiplicity counting, together with a knowledge of the gated efficiency of the neutron detector, makes it possible to deduce the ( $\gamma, n$ ), ( $\gamma, 2n$ ), and ( $\gamma, 3n$ ) cross sections. Further, it should be noted that this multiplicity technique allows one to take advantage of the fact that, for the first few MeV above the threshold for each of these reactions, the contribution of the bremsstrahlung photons to the number of multiple neutron counts is small relative to the contribution of the annihilation photons. Thus, for instance, the ( $\gamma, 2n$ ) cross section can be measured with high precision for a few MeV above its threshold even though the contribution of the positron bremsstrahlung to the total neutron yield at this energy is substantial, and a large subtraction must be made to obtain the ( $\gamma, n$ ) cross section there.

The efficiency of the neutron detector is about 40% after taking into account the small efficiency loss due to gating effects. It is also quite flat as a function of neutron energy, i.e., within 5% for these experiments. However, the outermost ring of BF<sub>3</sub> tubes is relatively more sensitive to high-energy neutrons than is the innermost,<sup>7</sup> since there is much more moderating material between the former and the neutron-producing sample than is the case for the latter. Hence, the ratio of the number of neutrons detected in the outermost to that in the innermost ring, the "ring ratio," varies with the average neutron energy. This fact allows one to determine the average neutron energy for a given sample material as a function of photon energy; and thus, in addition to the physics one learns from this observation, one can make any necessary corrections to the detector efficiency.

The calibration of the ring ratio as a function of neutron energy is shown in Fig. 1. The data were obtained from various monoenergetic ( $\gamma, n$ ) sources, radioactive ( $\alpha, n$ ) sources, a Cf<sup>252</sup> spontaneous-fission source, and from a portable ( $d+t$ ) neutron generator. The absolute detector efficiency as a function of neutron energy is shown in Fig. 2.

The efficiency used in the computation of the photoneutron cross sections thus is determined from Figs. 1

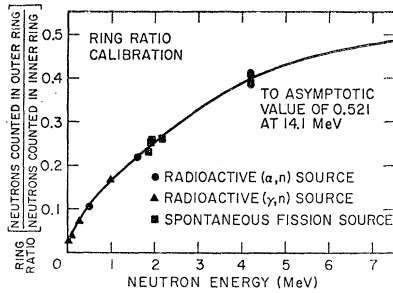


FIG. 1. Ring-ratio calibration as a function of neutron energy.

and 2 and from the actual ring ratio measured for each data point. In the cases where the samples were in oxide form, this method is not reliable above about 22 MeV. This results from the marked structure in the photoneutron cross section of oxygen in this energy range, together with the relatively high energy of the photoneutrons, both of which distort the measured ring ratio.<sup>7</sup> However, 22 MeV is well above the giant resonance in zirconium; and since the trend of the data is apparent, the relative uncertainty in the extrapolated efficiencies was judged to be not more than about 1%.

### III. ANALYSIS

For each isotope studied, the total photoneutron cross section  $\sigma[(\gamma, n) + (\gamma, pn) + (\gamma, 2n) + (\gamma, 3n) + \dots]$  and the various partial cross sections which make up this total cross section, namely,  $\sigma[(\gamma, n) + (\gamma, pn)]$ ,  $\sigma(\gamma, 2n)$ , and  $\sigma(\gamma, 3n)$ , have been calculated. No attempt has been made to separate the  $(\gamma, n)$  and  $(\gamma, pn)$  cross sections, since one neutron is emitted in both cases and besides, in all probability the  $(\gamma, pn)$  contribution is negligible in the giant-resonance region for these nuclei because of the Coulomb barrier.

In each case, a Lorentz-shaped curve computed from the formula

$$\sigma = \frac{\sigma_m}{1 + (E_\gamma^2 - E_m^2)^2 / E_\gamma^2 \Gamma^2}, \quad (1)$$

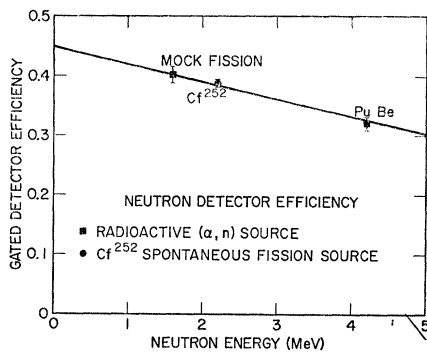


FIG. 2. Gated efficiency of the neutron detector as a function of neutron energy.

where  $\sigma_m$  is the peak cross section,  $E_m$  is the resonance energy, and  $\Gamma$  is the full resonance width at half-maximum, is fitted to the total photoneutron cross section. The details of the fit are not very sensitive to the energy region chosen within a few MeV; however, the lowest chi-squared values for the least-squares fitting procedure, as well as the best fits achieved by inspection, occurred when the fitting region was limited to 5 MeV about the giant resonance (14 to 19 MeV). These fits will be shown in the total-cross-section plots.

The ring-ratio data also are presented for each isotope in the form of plots of the ring ratio as a function of photon energy. The resulting neutron detector efficiency and neutron energy, obtained with the aid of Figs. 1 and 2, are shown on the ring-ratio plots. All the neutrons are included in these points so that the neutron energy measured by this technique is a weighted average of all neutrons from the neutron-producing reactions. The average neutron energy just above the  $(\gamma, 2n)$  threshold contains the weighting of the relative  $(\gamma, n)$  and  $(\gamma, 2n)$  cross sections and thus applies to neither reaction separately. At higher energies, however, the neutron yield results almost entirely from  $(\gamma, 2n)$  events, so that the ring-ratio technique gives the correct average neutron energy for  $(\gamma, 2n)$  neutrons. In the photon energy region above the giant resonance, the ring-ratio data begin to suffer severely from statistical considerations as well as from distortion owing to the presence of oxygen in those cases where the samples were in oxide form.

The integrated cross sections,  $\int \sigma dE$ , are determined from the data both for the total and partial cross sections for the energy regions over which data were taken. The areas under the Lorentz-curve fits are calculated from the formula

$$\text{Area} = \int_0^\infty \sigma dE_\gamma = \frac{1}{2} \pi \sigma_m \Gamma. \quad (2)$$

These values then can be compared with the prediction of the Thomas-Reiche-Kuhn (TRK) sum rule values of 0.06  $NZ/A$  MeV-b.

As was noted above, there is an uncertainty in the normalization which can lead to a systematic error in the measured cross sections. However, the effect of such an error is small, except for the single photoneutron cross-section measurements above the giant resonance, where the relatively small  $(\gamma, n)$  cross section is determined from the subtraction of one large number from another. This uncertainty is illustrated in the plots of  $\sigma[(\gamma, n) + (\gamma, pn)]$  by dashed lines. The maximum error introduced by this effect into the integrated total cross-section determination, however, in the worst case (that of  $Zr^{91}$ ) is less than 4%.

The threshold values for the various photoneutron reactions are shown in the plots by arrows. The threshold energies determined in the present experiment are

TABLE II. Photoneutron threshold values.

Nucleus	$E_{\text{thr}}(\gamma, n)$ (MeV)		$E_{\text{thr}}(\gamma, 2n)$ (MeV)		$E_{\text{thr}}(\gamma, 3n)$ (MeV)	
	a	b	a	b	a	b
$\text{Y}^{89}$	$11.48 \pm 0.01$	$11.5 \pm 0.1$	$20.7 \pm 0.2$	$20.8 \pm 0.1$	$33 \pm 1$	
$\text{Zr}^{90}$	$12.00 \pm 0.01$	$12.4 \pm 0.1^e$	$21.0 \pm 1.0$	$21.3 \pm 0.1$	$33 \pm 2$	
$\text{Zr}^{91}$	$7.194 \pm 0.005$		$19.19 \pm 0.01$	$19.1 \pm 0.1$	$28 \pm 1$	
$\text{Zr}^{92}$	$8.640 \pm 0.005$		$15.834 \pm 0.003$	$15.8 \pm 0.1$	$27.83 \pm 0.01$	
$\text{Zr}^{94}$	$8.20 \pm 0.01$	$8.0 \pm 0.2$	$14.948 \pm 0.003$	$15.0 \pm 0.1$	$23.59 \pm 0.01$	$24.5 \pm 1.0$

<sup>a</sup> Values given in Ref. 10.

<sup>b</sup> Measured in the present experiment.

<sup>c</sup> This represents the threshold for the  $\text{Zr}^{90}(\gamma, n)\text{Zr}^{89m}$  reaction (see Ref. 1), since the ground-state reaction requires a large change in angular momentum, and hence is inhibited strongly.

given in Table II, along with the values tabulated in Mattauch *et al.*<sup>10</sup>

## IV. RESULTS

### A. Ring-Ratio Data

The ring-ratio data for  $\text{Y}^{89}$ ,  $\text{Zr}^{90}$ ,  $\text{Zr}^{91}$ ,  $\text{Zr}^{92}$ , and  $\text{Zr}^{94}$  are presented in Figs. 3 through 7, respectively. The

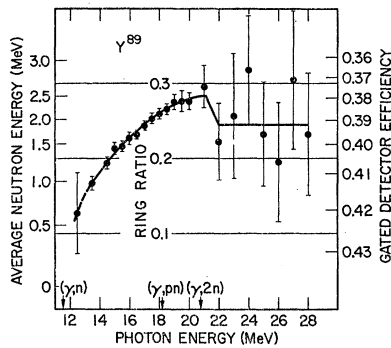


FIG. 3. Ring-ratio data for  $\text{Y}^{89}$  as a function of photon energy. The ordinate is the ring ratio (full scale is 0.40), and has been converted to read both average neutron energy and the neutron detector efficiency with the use of the plots in Figs. 1 and 2. Note the long slow rise above the  $(\gamma, n)$  threshold, the drop at the  $(\gamma, 2n)$  threshold, and the fact that the usefulness of the data above the giant resonance is reduced considerably by the poor statistics. The curve through the data represents the best fit from inspection, and was used to compute the detector efficiency for each data point in the cross-section analysis.

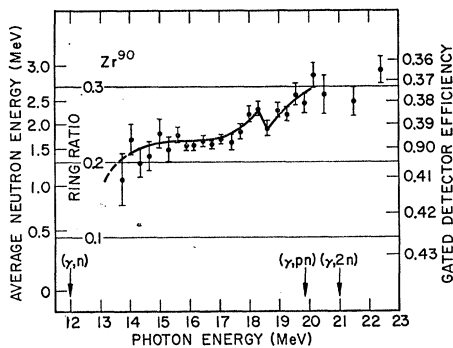


FIG. 4. Ring-ratio data for  $\text{Zr}^{90}$ . The dashed part of the curve represents extrapolation of the fitted curve into a region of poor statistics. Note the structure in the data, in particular, the sharp drop at 18.3 MeV.

<sup>10</sup> J. H. E. Mattauch, W. Thiele, and A. H. Wapstra, Nucl. Phys. 67, 32 (1965).

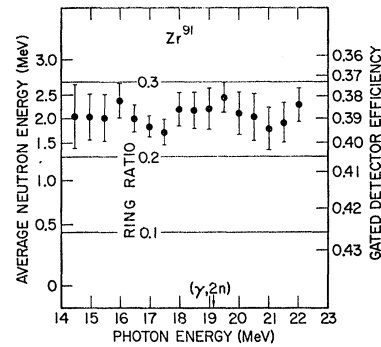


FIG. 5. Ring-ratio data for  $\text{Zr}^{91}$ .

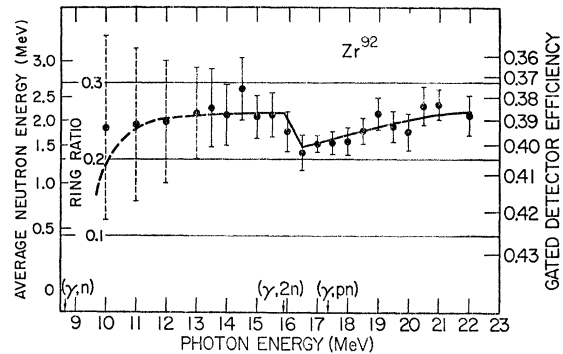


FIG. 6. Ring-ratio data for  $\text{Zr}^{92}$ . Note the sharp rise above the  $(\gamma, n)$  threshold. The dashed points were calculated from extrapolated curves in the threshold region.

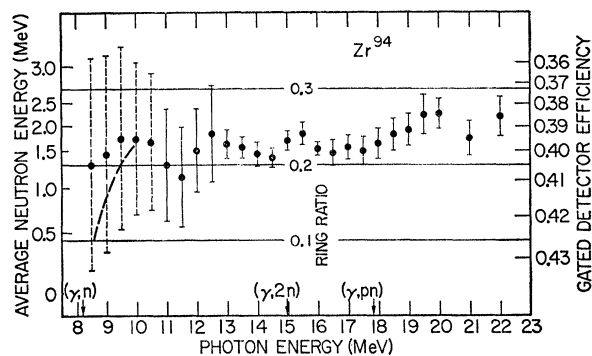


FIG. 7. Ring-ratio data for  $\text{Zr}^{94}$ . Note the sharp rise above the  $(\gamma, n)$  threshold, and that there is no pronounced dip above the  $(\gamma, 2n)$  threshold, despite the fact that there is a very large  $(\gamma, 2n)$  cross section.

$Y^{89}$  data (Fig. 3) are, in some respects, the most interesting. The photoneutron process in  $Y^{89}$  is characterized by a long slow rise of the average neutron energy over an 8-MeV region above the  $(\gamma, n)$  threshold, whereas the others rise more sharply to an asymptotic value, usually within a few MeV of the  $(\gamma, n)$  threshold. Furthermore, the onset of the giant resonance itself appears not to influence the character of this rise in neutron energy; an asymptote is not reached until the photon energy exceeds 20 MeV, and then  $(\gamma, 2n)$  events, together with poor statistics because of the diminishing cross section, make further interpretation difficult. Two factors which might influence the ring-ratio data are: (1)  $Y^{89}$  has a closed shell of 50 neutrons (in common with  $Zr^{90}$ ); and (2) the residual  $Y^{88}$  nucleus is odd-odd. In the case of the  $Zr^{90}$  ring-ratio data (Fig. 4), the dominant feature is the apparent structure. The average neutron energy is nearly constant throughout the giant-resonance region, and a sharp drop occurs just above 18.3 MeV. Since such a decrease in the ring ratio usually indicates the onset of a copious group of low-energy neutrons, there is the possibility that a new reaction channel is opening.

For the  $Zr^{91}$ ,  $Zr^{92}$ , and  $Zr^{94}$  cases (Figs. 5 through 7, respectively), the data are not so good as for the cases already discussed, owing partly to the samples being in oxide form and partly to their smaller mass. The  $Zr^{91}$  ring-ratio data (Fig. 5) are consistent with a constant average neutron energy throughout the energy range shown in the figure, and no structure is apparent at the  $(\gamma, 2n)$  threshold or elsewhere. On the other hand, the  $Zr^{92}$  ring-ratio data (Fig. 6), and hence the average neutron energy, show a sharp drop at the  $(\gamma, 2n)$  threshold, as one expects should the  $(\gamma, 2n)$  cross section be large and rise rapidly above its threshold. In the case of  $Zr^{94}$  (Fig. 7), it is apparent that the neutron energy increases sharply to an asymptotic value very close to the  $(\gamma, n)$  threshold. This is qualitatively different from the  $Y^{89}$  case, and might reflect the fact that the residual  $Zr^{93}$  nucleus is even-odd or that  $Zr^{94}$  is farther from the  $N=50$  closed neutron shell. It appears that  $Zr^{92}$  also shows this behavior; but the  $Zr^{91}$  data were judged to be not good enough to attempt such a low-energy extrapolation. Perhaps the most remarkable feature of the  $Zr^{94}$  data, however, is the fact that in spite of the very large  $(\gamma, 2n)$  cross section, the ring ratio shows no

pronounced dip at the  $(\gamma, 2n)$  threshold. Rather, it is almost constant throughout the energy range studied.

The neutron detector efficiency, as determined from the ring-ratio data and Figs. 1 and 2, is shown at the right of Figs. 3 through 7. Constant efficiency values were used to compute the cross sections for the  $Zr^{91}$  and  $Zr^{94}$  cases. Finally, the measured average neutron energies  $\bar{E}_n$  at the peaks of the giant resonances for the five nuclei are given in Table III. For an analysis of the data in terms of nuclear level densities, however, the average neutron energy for  $(\gamma, n)$  neutrons alone is required; but for  $Zr^{92}$  and  $Zr^{94}$ , the fact that the  $(\gamma, 2n)$  threshold lies below the peak of the giant resonance introduces an uncertainty in the assignment of this energy. For these cases,  $\bar{E}_n$  is obtained from an extrapolation of the ring-ratio data from below the  $(\gamma, 2n)$  threshold, up to the peak of the giant resonance.

## B. Cross-Section Data

The cross-section data for  $Y^{89}$ ,  $Zr^{90}$ ,  $Zr^{91}$ ,  $Zr^{92}$ , and  $Zr^{94}$  are presented in Figs. 8 through 12, respectively. The integrated cross-section data are presented in Table IV.

### 1. $Y^{89}$

The total photoneutron cross section for  $Y^{89}$  [Fig. 8(a)] exhibits the narrowest giant resonance ( $<4$  MeV) of any of the isotopes presented here. Also, some structure is apparent at 12.2 and 21 MeV, and possibly also at 22.5 and 25 MeV. The single photoneutron cross section [Fig. 8(b)] decreases to zero a few MeV above the  $(\gamma, 2n)$  threshold, as one expects from statistical theory. The  $(\gamma, 2n)$  cross section [Fig. 8(c)] has a high threshold, and reaches its maximum value of 18 mb at 23.3 MeV. The  $(\gamma, 2n)$  threshold value at  $20.8 \pm 0.1$  MeV measured here, together with the mass spectrographic data of Ries *et al.*,<sup>11</sup> determines the mass of  $Y^{87}$  to be  $86.91087 \pm 0.00011$  amu (the scale used is that for which 1 amu = 1/12 times the mass of  $C^{12} = 931.5$  MeV). This can be converted into a mass excess for  $Y^{87}$  of  $-83.0 \pm 0.1$  MeV, a value which now is determined with a precision somewhat higher than the value of  $-83.15 \pm 0.2$  MeV given in Mattauch *et al.*<sup>12</sup> Data were obtained from two samples of  $Y^{89}$ , whose masses were about 300 and 460 g. Two separate determinations of the absolute cross section in the giant-resonance region were made with the 300-g sample, which was wholly within the central part of the photon beam. The data taken with the large sample were normalized to the data taken with the smaller, but this necessitated a correction of only 5%. The uncertainty in the absolute cross section resulting from this procedure is less than 1%. The  $(\gamma, 3n)$  thresholds for  $Y^{89}$  and  $Zr^{90}$  occur at a photon energy of about 33 MeV, above the range of the present data.

<sup>11</sup> R. R. Ries, R. A. Damerow, and W. H. Johnson, Jr., *Phys. Rev.* **132**, 1662 (1963).

<sup>12</sup> J. H. E. Mattauch, W. Thiele, and A. H. Wapstra, *Nucl. Phys.* **67**, 1 (1965).

TABLE III. Average neutron energy at  $E_\gamma = E_m$ .

Nucleus	$\bar{E}_n$ (MeV)
$Y^{89}$	$1.9 \pm 0.1$
$Zr^{90}$	$1.7 \pm 0.1$
$Zr^{91}$	$2.1 \pm 0.1$
$Zr^{92}$	$1.7 \pm 0.1^a$
$Zr^{94}$	$1.6 \pm 0.1^b$

<sup>a</sup>  $2.2 \pm 0.2$  MeV for  $(\gamma, n)$  neutrons alone.

<sup>b</sup>  $2.0 \pm 0.4^{+0.2}$  MeV for  $(\gamma, n)$  neutrons alone.

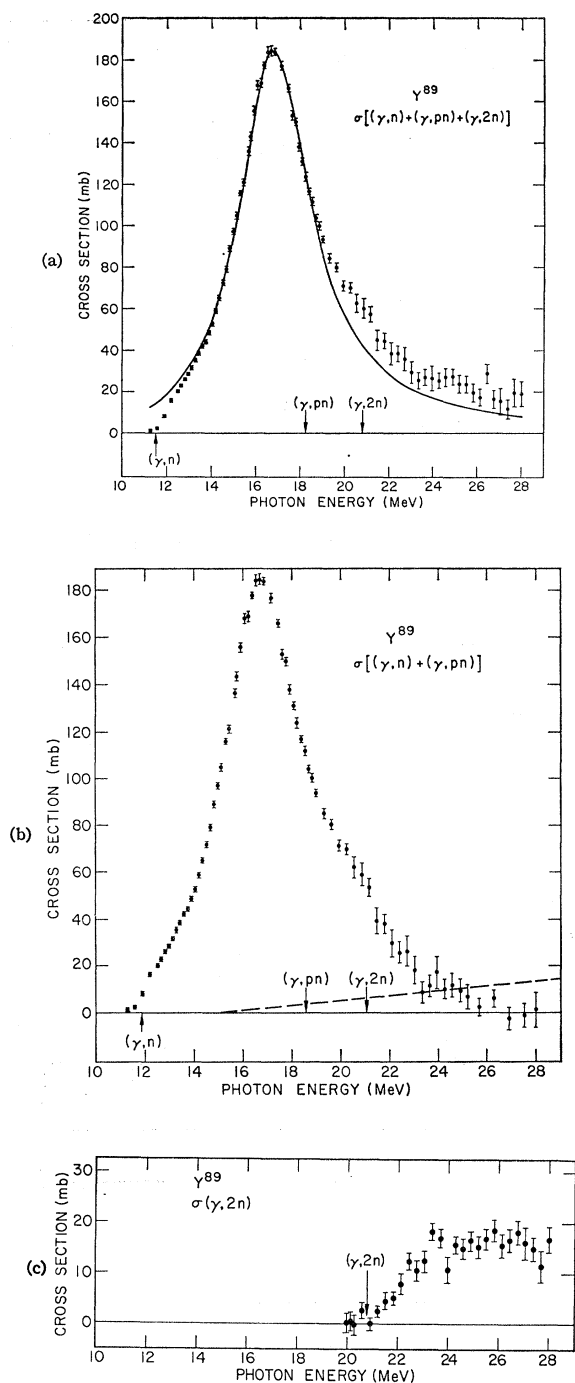


FIG. 8 (a) Total photoneutron cross section  $\sigma[(\gamma,n) + (\gamma,pn) + (\gamma,2n)]$  for  $Y^{89}$ . The solid curve is a Lorentz-line fit to the giant-resonance data (14 to 19 MeV). The thresholds (arrows), except when otherwise noted, are from Ref. 10. In this case, the  $(\gamma,2n)$  threshold is taken from the data. (b) Single photoneutron cross section  $\sigma[(\gamma,n) + (\gamma,pn)]$  for  $Y^{89}$ . The dashed line represents the maximum possible systematic error owing to the uncertainty in the normalization constant for the bremsstrahlung subtraction (see text). (c) The  $(\gamma,2n)$  cross section for  $Y^{89}$ . The threshold determination of  $20.8 \pm 0.1$  MeV determines the mass of  $Y^{87}$  (see text). The threshold value is taken from the data. The cross-section scale has been doubled for clarity.

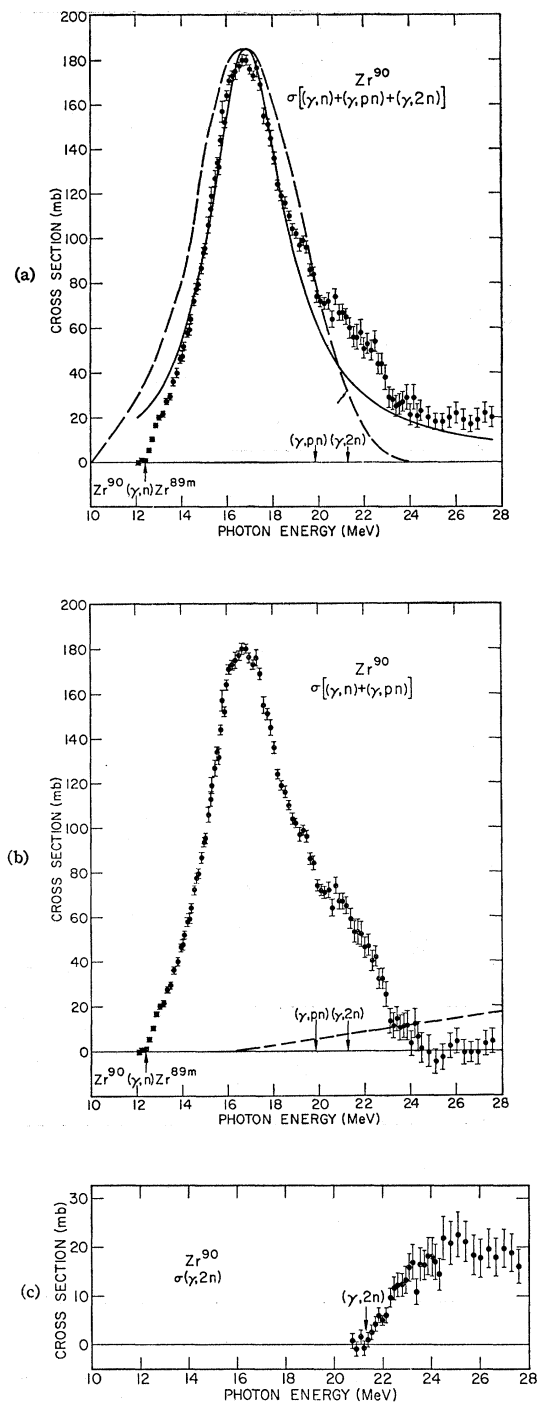


FIG. 9 (a) Total photoneutron cross section for  $Zr^{90}$ . The dashed curve is the theoretical prediction of a shell-model calculation by Shitikova and co-workers, (Refs. 13 and 14) normalized both in energy and in cross section to the present data. The predicted giant resonance is too broad, and falls off too rapidly at high energies. Balashov and Yadrovsky (Ref. 15) also have done a particle-hole calculation for  $Zr^{90}$ , but here the giant resonance occurs at too low an energy ( $\approx 15$  MeV). The  $(\gamma,n)$  and  $(\gamma,2n)$  thresholds are taken from the data. (b) Single photoneutron cross section for  $Zr^{90}$ . (c) The  $(\gamma,2n)$  cross section for  $Zr^{90}$ . The threshold determination of  $21.3 \pm 0.1$  MeV determines the mass of  $Zr^{88}$  (see text).

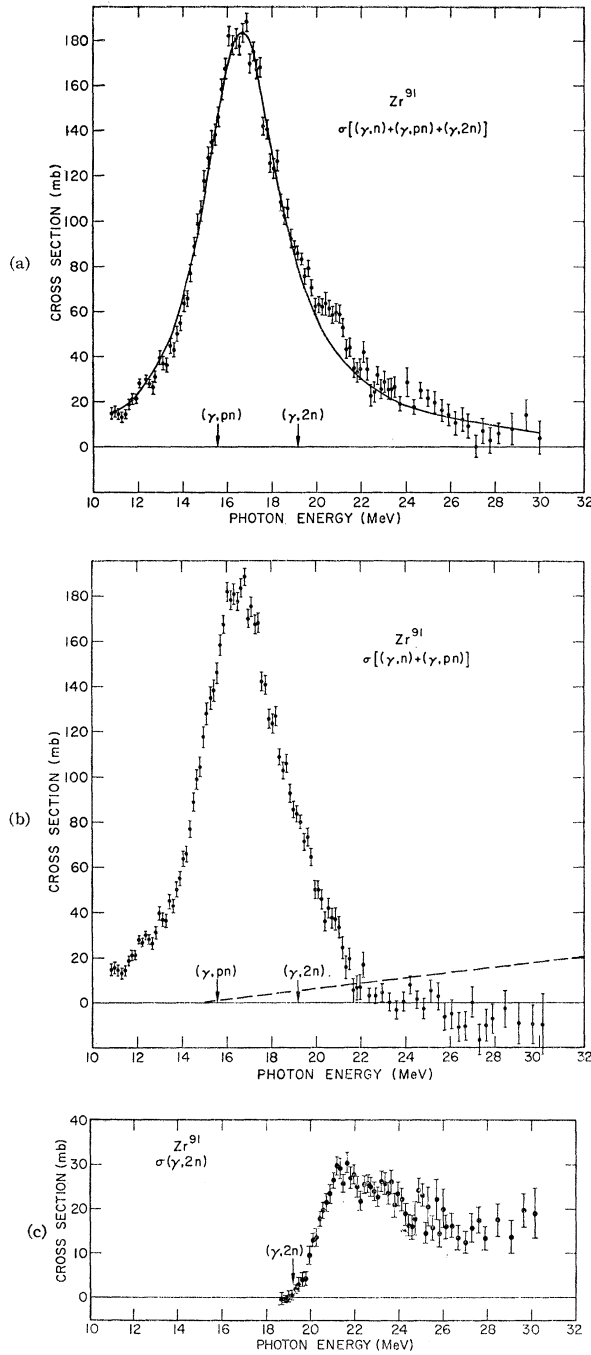


FIG. 10. (a) Total photoneutron cross section for  $Zr^{91}$ . (b) Single photoneutron cross section for  $Zr^{91}$ . (c) The  $(\gamma,2n)$  cross section for  $Zr^{91}$ .

## 2. $Zr^{90}$

For the case of  $Zr^{90}$  two samples were used, one metallic and the other oxide, whose masses were about 200 and 70 g, respectively. Like  $Y^{89}$ ,  $Zr^{90}$  has a closed shell of 50 neutrons. The total photoneutron cross section [Fig. 9(a)] again exhibits a narrow giant reso-

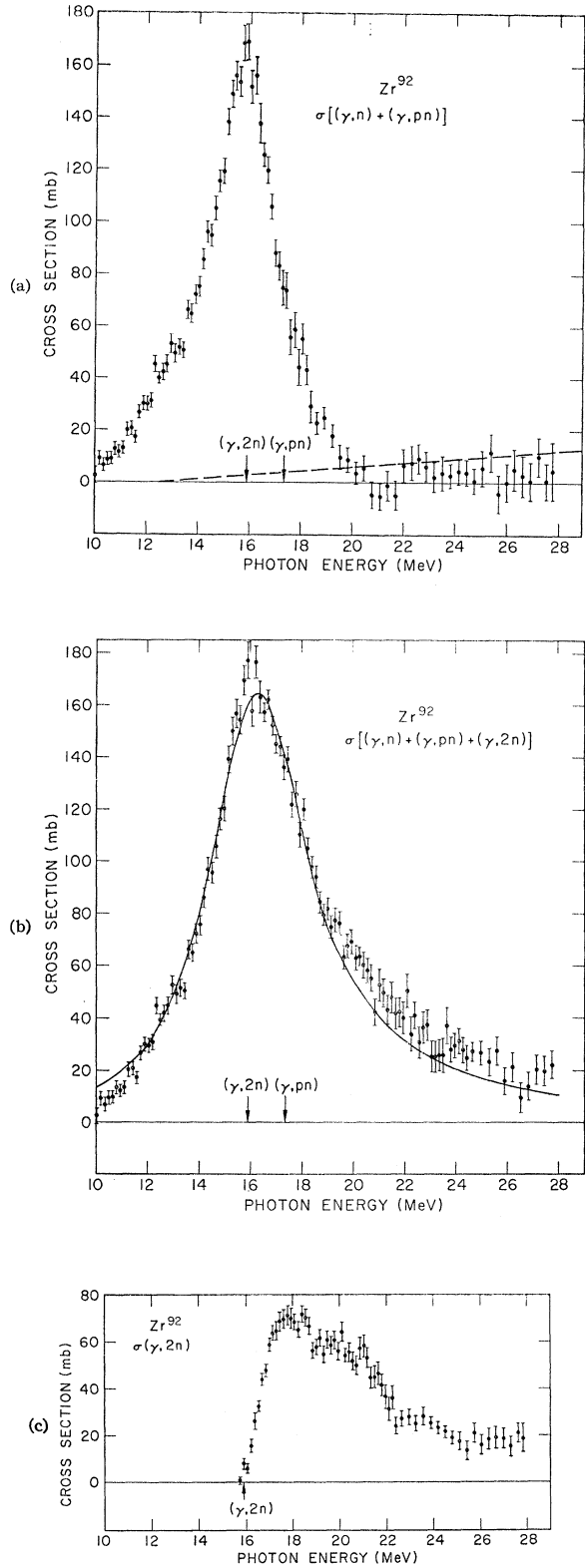


FIG. 11. (a) Total photoneutron cross section for  $Zr^{92}$ . (b) Single photoneutron cross section for  $Zr^{92}$ . (c) The  $(\gamma,2n)$  cross section for  $Zr^{92}$ .

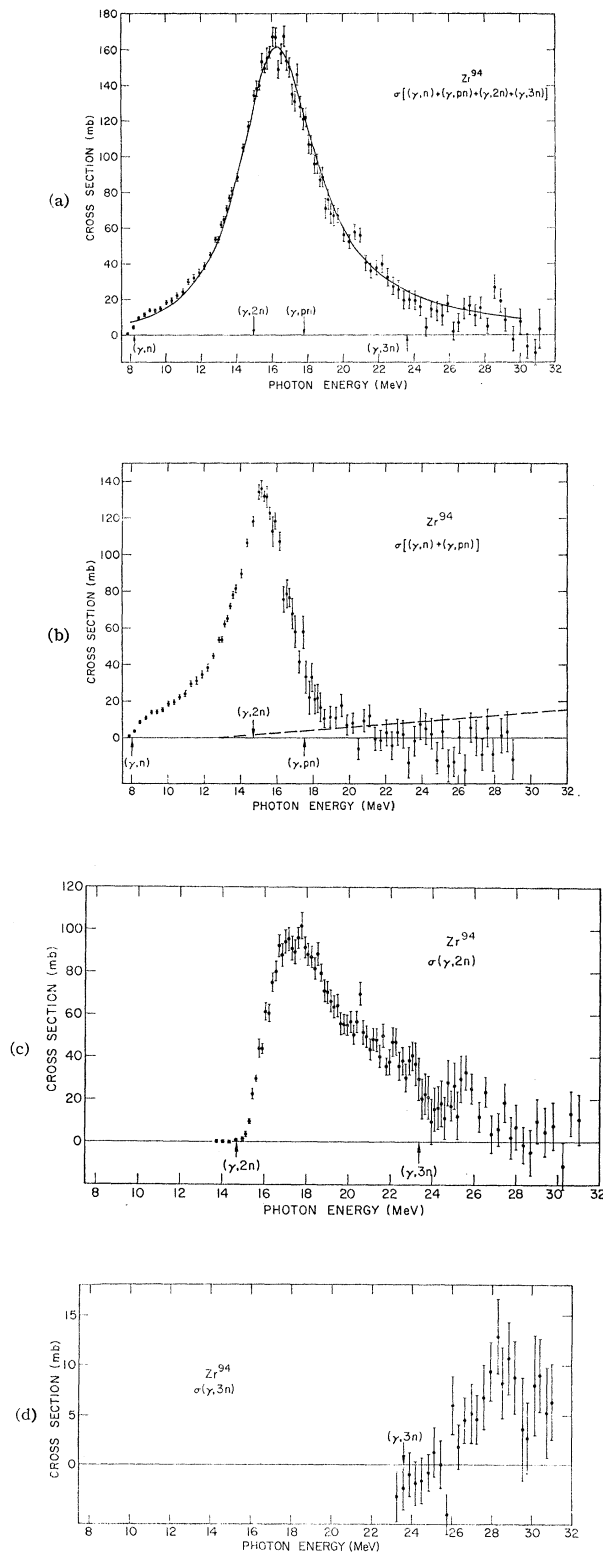


FIG. 12. (a) Total photoneutron cross section  $\sigma[(\gamma,n) + (\gamma,pn) + (\gamma,2n) + (\gamma,3n)]$  for  $Zr^{94}$ . (b) Single photoneutron cross section for  $Zr^{94}$ : (c) The  $(\gamma,2n)$  cross section for  $Zr^{94}$ . (d) The  $(\gamma,3n)$  cross section for  $Zr^{94}$ .

nance. The dashed curve is the theoretical prediction of Shitikova *et al.*<sup>13,14</sup> Balashov and Yadvovsky<sup>15</sup> also have done a calculation for  $Zr^{90}$ , but their prediction of the giant-resonance energy is too low. Structure appears at 13 MeV, and also in the energy region between 19 and 23 MeV. The latter probably consists of two or three peaks; the onset of this structure at 19 MeV might be correlated with the decrease in the average neutron energy at about 18.5 MeV (see Fig. 4). Both this rise in the photoneutron cross section and this decrease in the average neutron energy occurred in measurements made with both samples. The  $(\gamma,2n)$  cross section rises to its maximum of 22 mb at 25.1 MeV. The  $(\gamma,2n)$  threshold measurement of  $21.3 \pm 0.1$  MeV, together with the mass spectrographic data,<sup>11</sup> determines the mass of  $Zr^{88}$  to be  $87.91023 \pm 0.00011$  amu, which can be converted into a mass excess for  $Zr^{88}$  of  $-83.6 \pm 0.1$  MeV. This value is considerably better than the value of  $-83.77 \pm 1.0$  MeV given in Ref. 12.

### 3. $Zr^{91}$

The separated  $Zr^{91}$ ,  $Zr^{92}$ , and  $Zr^{94}$  samples were in oxide form; the mass of each was about 55 g. The  $Zr^{91}$  cross sections also have the same general character as those for the above closed-neutron-shell nuclei, except for the shift to a slightly lower resonance energy and somewhat larger width. There is structure in the total photoneutron cross section [Fig. 10(a)] at 12.3 and 20.6 MeV; the latter peak is about 1.3 MeV broad at its base. For  $Zr^{91}$ , the single photoneutron cross section [Fig. 10(b)] appears to go negative for photon energies above 26 MeV. This behavior probably results from the uncertainty in the subtraction of the neutron counts caused by the positron bremsstrahlung, as was mentioned above. The dashed line in the figure represents the magnitude of this uncertainty; it can be seen that this cross section is consistent with zero in this energy range. There is a large (12-MeV) gap between the  $(\gamma,n)$  and  $(\gamma,2n)$  thresholds for this nucleus; data were not taken all the way down to the lower threshold, and the upper one is not very much lower than that for  $Zr^{90}$ . The  $(\gamma,2n)$  cross section [Fig. 10(c)], although somewhat larger than that for  $Zr^{90}$ , rises to a maximum of only 29 mb at 21.3 MeV, and then decreases somewhat. The 3.3%  $Zr^{92}$  contamination of the  $Zr^{91}$  sample was taken into account in the energy region above the  $(\gamma,2n)$  threshold, and necessitated a correction to the  $(\gamma,2n)$  cross section for  $Zr^{91}$  of 2 mb. The data above the  $(\gamma,3n)$  thresholds for  $Zr^{91}$  and  $Zr^{92}$  at about 28 MeV were insufficient to extract meaningful  $(\gamma,3n)$  cross sections.

<sup>13</sup> K. V. Shitikova, Zh. Eksperim. i Teor. Fiz. **42**, 868 (1962) [English transl.: Soviet Phys.—JETP **15**, 603 (1962)].

<sup>14</sup> B. S. Ishkhanov, K. V. Shitikova, and B. A. Yur'ev, Bull. Acad. Sci. USSR **29**, 216 (1965).

<sup>15</sup> V. V. Balashov and E. L. Yadvovsky, Phys. Letters **22**, 509 (1966).

TABLE IV. Integrated cross sections.

Nucleus	$\sigma_{\text{int}}[(\gamma, n) + (\gamma, pn)]$ (MeV-b) <sup>a</sup>	$\sigma_{\text{int}}(\gamma, 2n)$ (MeV-b) <sup>a</sup>	$E_{\gamma\text{max}}$ (MeV)	$\frac{\sigma_{\text{int}}(\gamma, 2n)}{\sigma_{\text{int}}(\gamma, \text{total})}$ <sup>b</sup>	$(\frac{1}{2}\pi)\sigma_m\Gamma$ (MeV-b)	$0.06NZ/A$ (MeV-b)
Y <sup>89</sup>	0.94	0.10	28	0.10	1.14	1.31
Zr <sup>90</sup>	0.96	0.10	28	0.09	1.16	1.33
Zr <sup>91</sup>	0.88	0.20	30	0.19	1.22	1.35
Zr <sup>92</sup>	0.65	0.45	28	0.41	1.23	1.36
Zr <sup>94</sup>	0.43	0.58	30	0.56 <sup>c</sup>	1.32	1.38

<sup>a</sup> All measured integrated cross-section values are given for an energy region from threshold to  $E_{\gamma\text{max}}$ . For the Zr<sup>91</sup> and Zr<sup>92</sup> cases, it was necessary to extrapolate the low-energy part of the total photoneutron cross section down to threshold; the error introduced in this process, however, is less than 0.5%.  
<sup>b</sup> The word "total" in this table refers to the total photoneutron cross section  $\sigma[(\gamma, n) + (\gamma, pn) + (\gamma, 2n) + (\gamma, 3n)]$ , and excludes the  $(\gamma, \gamma)$  and  $(\gamma, p)$  cross sections.

<sup>c</sup> This value includes the contribution of  $\sigma_{\text{int}}(\gamma, 3n)$ , which equals 0.03 MeV-b from threshold to 30 MeV.

#### 4. Zr<sup>92</sup>

The character of the photoneutron cross sections for Zr<sup>92</sup> is markedly different from those for the preceding three nuclei. The  $(\gamma, 2n)$  cross section [Fig. 11(c)] has a threshold at 15.8 MeV, and rises to its maximum value of 71 mb at 17.8 MeV. The giant resonance [see Fig. 11(a)] is broader (4.7 MeV) and the peak cross section is lower ( $\approx 170$  mb, as opposed to 185 mb for the three cases above). The single photoneutron cross section [Fig. 11(b)] drops precipitously from about 170 mb to zero within 4 MeV. Also, there are sugges-

tions of structure at 12 and 13 MeV, as well as in the energy range from 19 to 22 MeV, the last being most apparent in the  $(\gamma, 2n)$  cross section.

#### 5. Zr<sup>94</sup>

The case of Zr<sup>94</sup> is even more extreme, when compared with Y<sup>89</sup> and Zr<sup>90</sup>. The giant resonance in the total photoneutron cross section [Fig. 12(a)] has a peak value of about 165 mb at 16.2 MeV, and has a width of 5.2 MeV. Like Zr<sup>92</sup>, it occurs at a lower energy, has a lower peak cross section, and has larger width than the others. For Zr<sup>94</sup> the  $(\gamma, 2n)$  threshold actually is appreciably below the peak of the giant resonance, and the resulting takeover of the dipole strength by this decay mode is striking. The single photoneutron cross section [Fig. 12(b)] peaks at 15.1 MeV at a value of less than 140 mb, and drops to less than 20 mb within 3 MeV. The  $(\gamma, 2n)$  cross section shown in Fig. 12(c) achieves a value of almost 100 mb within 2 MeV of its threshold, which is 15.0 MeV. This nucleus is a clear case for which a measurement of the  $(\gamma, n)$  cross section alone would give too small and narrow a giant resonance, centered at too low a photon energy, while a total neutron yield measurement would err in the opposite direction; the multiplicity feature of the present experiment is essential in order to discern the true picture. The  $(\gamma, n)$  threshold is determined here to be located at  $8.0 \pm 0.2$  MeV, compared with the value of  $8.20 \pm 0.01$  MeV in Ref. 12. The relatively large uncertainty in the present determination of this threshold results from having taken the data in the low-energy region with wider slit settings for the energy analysis of the positron beam, which was made necessary by the low positron yield from the accelerator at this energy. Structure is apparent at 9.1 MeV, and perhaps also in the  $(\gamma, 2n)$  cross section in the energy range of 20 to 23 MeV. Finally, some data were acquired for the  $(\gamma, 3n)$  cross section [Fig. 12(d)], and it is interesting that, in keeping with statistical theory, this decay mode in turn becomes dominant shortly above its threshold. Furthermore, the  $(\gamma, 3n)$  cross section is beginning to fall off at the highest energies, as one expects should the total photoneutron cross section follow a Lorentz shape.

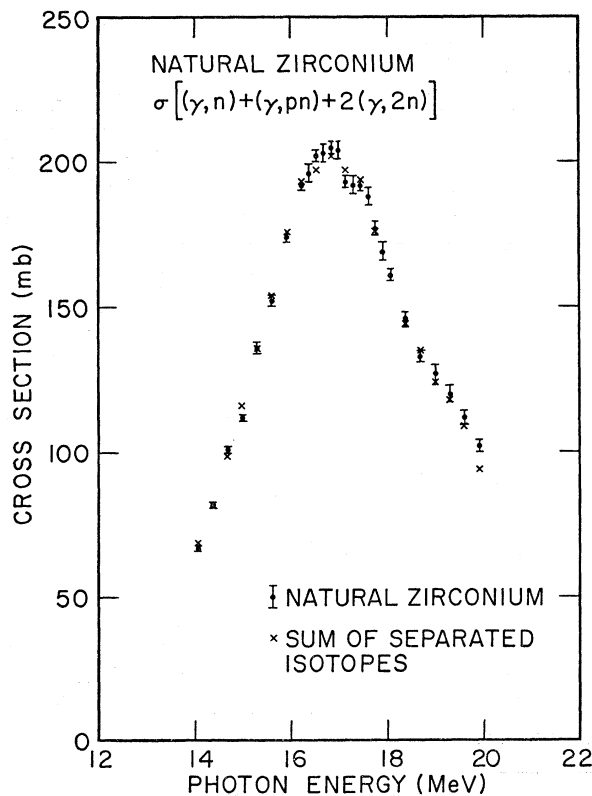


FIG. 13. Photoneutron yield cross section  $\sigma[(\gamma, n) + (\gamma, pn) + 2(\gamma, 2n)]$  for natural zirconium (points with error bars), compared with the sum of the yield cross sections for the separated zirconium isotopes, weighted by their natural isotopic abundances (crosses). No normalization of the data has been performed.

## 6. Natural Zirconium

In addition to the data presented for the separated zirconium isotopes, measurements were made with a sample of natural zirconium whose mass was about 210 g. The resulting neutron yield data in the giant-resonance region are compared with the sum of the yield cross sections for the separated isotopes, weighted by their natural isotopic abundances, in Fig. 13. The cross section for the 2.8%-abundant  $Zr^{96}$  isotope is estimated as if it has the same shape as the  $Zr^{94}$  cross section. The fact that the  $Zr^{96}$  ( $\gamma, 2n$ ) threshold is 0.7 MeV lower than that for  $Zr^{94}$  introduces an uncertainty of considerably less than 1%. As can be seen in the figure, the agreement between the sum of the cross sections for the separated isotopes and that for the natural zirconium is excellent. This shows that the present cross-section measurements for the zirconium isotopes are consistent with regard to both absolute value and shape, at least in the giant-resonance region.

## V. DISCUSSION

## A. Giant-Resonance Parameters

The parameters of the Lorentz curves fitted to the total photoneutron cross sections are given in Table V. In contrast to the data of Ref. 3 shown in Table VI, all the parameters of the giant resonance show a regular progression with the atomic weight.

The resonance energy  $E_m$  varies as some gentle function of the mass number  $A$ , and it is known that this variation persists throughout most of the periodic table.<sup>16</sup> This variation can be used to test the classical models based on the collective motion of the protons and neutrons inside the nucleus put forward by Goldhaber and Teller<sup>17</sup> and by Steinwedel and Jensen.<sup>18</sup> In one model,<sup>17</sup> the resonance energy is proportional to  $A^{-1/6}$ , and in another,<sup>17,18</sup> to  $A^{-2/3}$ . The constants of proportionality appropriate to these two theories are given in Table VII. As can be seen from the table, there is little to choose between the two theories on the basis of the present data alone, since the range of  $A$  represented here is small.

The variation of the width of the giant resonance  $\Gamma$  shows the importance of the closed neutron shell. The closed-shell nuclei  $Y^{89}$  and  $Zr^{90}$  have resonances only about 4-MeV wide, but the width increases to 5.2 MeV for  $Zr^{94}$ , for which four additional neutrons have been added.

The resonance energies and widths also can be used to compute the nuclear symmetry parameter  $K$  which also appears, for example, in the Weizsäcker semi-

TABLE V. Parameters of Lorentz-curve fits to the giant resonance.<sup>a</sup>

Nucleus	$E_m$ (MeV)	$\sigma_m$ (mb)	$\Gamma$ (MeV)
$Y^{89}$	16.79±0.04	185±5	3.95±0.06
$Zr^{90}$	16.83±0.04	185±5	4.00±0.06
$Zr^{91}$	16.57±0.04	184±5	4.23±0.06
$Zr^{92}$	16.27±0.04	165±4	4.73±0.06
$Zr^{94}$	16.20±0.04	161±4	5.20±0.06

<sup>a</sup> The uncertainties for  $\sigma_m$  given here are relative. The absolute uncertainties are less than 12 mb.

empirical mass formula. According to Danos,<sup>19</sup>

$$E_m = \frac{\hbar k}{A} \left\{ \frac{8KNZ}{M} \left[ 1 - \left( \frac{\Gamma}{2E_m} \right)^2 \right] \right\}^{1/2}, \quad (3)$$

where  $kR=2.082$  for spherical nuclei, and  $R$  is the nuclear radius. The values for  $K$  are very nearly the same, as can be seen in Table VII, and agree with the value of 23 MeV obtained from mass analysis.<sup>20</sup> However, they are about 4 MeV smaller than the values for

TABLE VI. Giant-resonance parameters from Yergin and Fabricand.<sup>a,b</sup>

Nucleus	$E_m$ (MeV)	$\sigma_m$ (mb)	$\Gamma$ (MeV)	$\sigma_{int}$ (MeV-b)
$Y^{89}$	16.3	191	3.8	0.87
$Zr^{90}$	15.8	199	4.3	0.98
$Zr^{91}$	16.5	200	5.0	1.22
$Zr^{92}$	16.9	193	5.5	1.24

<sup>a</sup> See Ref. 3.

<sup>b</sup> The term  $\sigma_{int}$  is  $\int \sigma dE$ , where the limits of integration are from threshold to 23 MeV.

heavier nuclei (see Ref. 4 for a more complete discussion of the nuclear symmetry problem).

Furthermore, an important aspect of this analysis is that the parameters of the Lorentz fits were found to be quite insensitive to the photon energy range used in the fitting procedure. This fact is in excellent agreement with the classical collective description of the dipole photon absorption process.

TABLE VII. Parameters for classical theories.

Nucleus	$\alpha$ (MeV) <sup>a</sup>	$\beta$ (MeV) <sup>b</sup>	$K$ (MeV) <sup>c</sup>
$Y^{89}$	75.0	35.5	23.0
$Zr^{90}$	75.4	35.6	23.2
$Zr^{91}$	74.6	35.2	22.7
$Zr^{92}$	73.6	34.6	22.2
$Zr^{94}$	73.6	34.5	22.6
Average	74.4	35.1	22.7

<sup>a</sup>  $\alpha$  is the hydrodynamic parameter defined by  $E_m = \alpha A^{-1/3}$ .

<sup>b</sup>  $\beta$  is the collective parameter defined by  $E_m = \beta A^{-1/6}$ .

<sup>c</sup>  $K$  is the nuclear symmetry parameter defined by Eq. (3) in the text, where  $R_0=1.20$  F and  $Mc^2=931.5$  MeV, whence

$$K = 9.922 \times 10^{-4} (A^{8/3}/NZ) \frac{E_m^2}{1 - (\Gamma/2E_m)^2}.$$

<sup>16</sup> J. Levinger, *Nuclear Photo-Disintegration* (Oxford University Press, New York, 1960), p. 35.

<sup>17</sup> M. Goldhaber and E. Teller, *Phys. Rev.* **74**, 1046 (1948).

<sup>18</sup> H. Steinwedel and J. H. D. Jensen, *Z. Naturforsch.* **5a**, 413 (1950).

<sup>19</sup> M. Danos, *Nucl. Phys.* **5**, 23 (1958), in which there is a typographical error.

<sup>20</sup> A. E. S. Green, *Phys. Rev.* **95**, 1006 (1954).

### B. Integrated Cross Sections

The integrated cross sections are summarized in Table IV. The integrated total photoneutron cross section is typically 1.07 MeV-b integrated from threshold to 29 MeV, or 0.79 of the TRK sum rule value. Adding to this the integrated  $(\gamma, p)$  cross-section value for natural zirconium of 0.13 MeV-b,<sup>21</sup> or 0.10 of the sum rule value, one finds that about 11% of the dipole strength expected is still unaccounted for. Presumably, the missing strength occurs at higher energies, and an estimate of its magnitude can be made from the integrated cross sections derived from the Lorentz-curve fits (see Table IV). The sum of the areas under the Lorentz curves and the integrated  $(\gamma, p)$  cross section agree, within experimental limits, with the TRK value. It should be emphasized that it appears unnecessary to invoke any exchange-force effects to account for the observed dipole strength, in keeping with previous results obtained at this laboratory.<sup>22</sup> The integrated  $(\gamma, 2n)$  cross section increases rapidly as one adds neutrons to the closed shell; indeed, this quantity becomes the most important contributor to the integrated total cross section for Zr<sup>94</sup>. The ratio of  $\sigma_{\text{int}}(\gamma, 2n)$  to  $\sigma_{\text{int}}(\gamma, \text{total})$  is tabulated to display this effect. Systematic errors in the absolute cross sections, and hence in the integrated cross-section values presented here, do not exceed 7%; the relative precision of the values quoted, however, is better than 3%.

The integrated moments of the measured photoneutron cross sections  $\sigma_{-1}$  and  $\sigma_{-2}$  are given in Table VIII. Theoretical calculations by Levinger and others<sup>23</sup> predict that  $\sigma_{-1}$  be proportional to  $A^{4/3}$ . If so, the present measurements yield a proportionality constant of about 0.16 mb, in marked disagreement with the values of 0.30 and 0.36 mb given in Ref. 23. The  $\sigma_{-2}$  data probably have greater importance since  $\sigma_{-2}$  is proportional to the nuclear polarizability. In particular,<sup>24</sup>

$$\sigma_{-2} = \frac{\pi^2 e^2 R^2 A}{20 hc K}, \quad (4)$$

where  $R$  is the nuclear radius and  $K$  is the nuclear symmetry energy mentioned above. For  $R = 1.2A^{1/3}$  F, this reduces to  $0.05175A^{5/3}/K$  mb-MeV<sup>-1</sup>, if  $K$  is in MeV; and for  $K = 23$  MeV,<sup>20</sup>  $\sigma_{-2} = 0.00225A^{5/3}$  mb-MeV<sup>-1</sup>. It can be seen from Table VIII that the experimental values fall within 13% of this prediction. Moreover, if instead of the constant 23 MeV one uses the values for  $K$  given in Table VII, the seventh column in Table VIII shows that there is equally good agreement in this case. Finally, if one uses the measured values for  $\sigma_{-2}$  to

<sup>21</sup> I. I. Dushkov, B. S. Ishkhanov, I. M. Kapitonov, B. A. Yur'ev, and V. G. Shevchenko, *Phys. Letters* **10**, 310 (1964).

<sup>22</sup> S. C. Fultz, University of California, Lawrence Radiation Laboratory Report No. UCRL-70002, presented at the International Conference on Nuclear Physics, Gatlinburg, Tennessee, 1966 (to be published).

<sup>23</sup> Reference 16, p. 54.

<sup>24</sup> Reference 16, p. 51.

compute new values for the nuclear symmetry energy, which are given in the last column of Table VIII, the results, which average 24.4 MeV, are in somewhat better agreement with the values typical of heavier elements given in Ref. 4.

### C. Nuclear Level Densities

Another kind of nuclear information which can be extracted from the data is the determination of the nuclear level density in the range of excitation energy a few MeV above the  $(\gamma, n)$  threshold in nuclei. The ratio of the  $(\gamma, 2n)$  to the total photoneutron cross section just above the  $(\gamma, 2n)$  threshold in the target nucleus gives the level density in the nucleus having one neutron less than the target nucleus at the appropriate excitation energy  $U$ , according to the formula

$$\frac{\sigma(\gamma, 2n)}{\sigma(\gamma, \text{total})} = \frac{\int_0^{E_\gamma - E_{\text{thr}}(\gamma, 2n)} \rho(U) E_n dE_n}{\int_0^{E_\gamma - E_{\text{thr}}(\gamma, n) - \Delta} \rho(U) E_n dE_n}. \quad (5)$$

Here the excitation energy  $U = E_\gamma - E_{\text{thr}}(\gamma, n) - E_n - \Delta$ ;  $\Delta$  is a correction to the ground state of the target-minus-one-neutron nucleus from shell and pairing effects;  $\rho$  is the density of states; and it is assumed that the inverse neutron absorption cross section is constant. Considerable attention has been given to the determination of the proper form for the density of states, and there is considerable disagreement on the subject. The functional form of  $\rho$  is given by Ericson<sup>25</sup> as

$$\rho \propto U^{-2} \exp[2(aU)^{1/2}] \quad (6)$$

and by Blatt and Weisskopf<sup>26</sup> as

$$\rho \propto \exp[2(aU)^{1/2}], \quad (7)$$

where  $a$  is the nuclear level density parameter.

The analysis was carried out with the use of both Eqs. (6) and (7). A parameter search was conducted for  $a$  and  $\Delta$ , using a least-squares fitting technique for the ratio  $\sigma(\gamma, 2n)/\sigma(\gamma, \text{total})$  in the appropriate photon energy range. Finally, the average energy  $\bar{E}_n$  of the first neutron emitted in the  $(\gamma, 2n)$  process was computed from the formula

$$\bar{E}_n = \frac{\int_0^{E_\gamma - E_{\text{thr}}(\gamma, n) - \Delta} \rho(U) E_n^2 dE_n}{\int_0^{E_\gamma - E_{\text{thr}}(\gamma, n) - \Delta} \rho(U) E_n dE_n}. \quad (8)$$

This average energy now can be compared with the results of the ring-ratio measurements for the average

<sup>25</sup> T. Ericson, *Advan. Phys.* **9**, 425 (1960).

<sup>26</sup> J. M. Blatt and V. F. Weisskopf, *Theoretical Nuclear Physics* (John Wiley & Sons, Inc., New York, 1952), p. 379.

TABLE VIII. Integrated moments<sup>a</sup> of the measured photoneutron cross sections and sum rules.

Nucleus	$E_{\gamma\max}$ (MeV)	$\sigma_{-1}$ (mb)	$\sigma_{-1}A^{-4/3}$ (mb)	$\sigma_{-2}$ (mb-MeV <sup>-1</sup> )	$\sigma_{-1}$	$\sigma_{-2}K$	$0.05175A^{5/3}$
					$0.00225A^{5/3}$	$0.05175A^{5/3}$	$\sigma_{-2}$ (MeV)
Y <sup>89</sup>	28.0	59.9	0.151	3.48	0.87	0.87	26.3
Zr <sup>90</sup>	27.5	59.1	0.147	3.38	0.83	0.84	27.7
Zr <sup>91</sup>	30.0	65.6	0.160	4.08	0.99	0.98	23.3
Zr <sup>92</sup>	27.5	64.7	0.156	3.97	0.94	0.91	24.4
Zr <sup>94</sup>	31.0	69.2	0.162	4.44	1.02	1.00	22.6

<sup>a</sup>  $\sigma_{-1} = \int_{E_{\text{thr}}}^{E_{\gamma\max}} \sigma E^{-1} dE$  and  $\sigma_{-2} = \int_{E_{\text{thr}}}^{E_{\gamma\max}} \sigma E^{-2} dE$ , where  $\sigma$  is the total photoneutron cross section.

neutron energy at the peak of the giant resonance given in Table III. From this quantity and the  $\chi^2$  values for the least-square fits mentioned above, the best pair of values for  $a$  and  $\Delta$  are determined. For example, Fig. 14 shows the ratio of the  $(\gamma, 2n)$  cross section to the total photoneutron cross section for Zr<sup>91</sup> plotted as a function of photon energy. The solid line is the curve generated by Eq. (5) for  $a=4.0$  MeV<sup>-1</sup> and  $\Delta=5.0$  MeV when Eq. (7) is used for the density of states. These values for  $a$  and  $\Delta$  were chosen so that Eq. (8) gives the value of  $\bar{E}_n=2.1$  MeV for a photon energy  $E_\gamma = E_m=16.57$  MeV, to agree with the ring-ratio value for  $\bar{E}_n$  given in Table III.

The results of this analysis are given in Table IX. The lower and upper limits of the range of excitation energy  $U$ , denoted by  $U_<$  and  $U_>$ , respectively, are given in columns 3 and 4 of the table, and refer to the target-minus-one-neutron nucleus with no shift of its ground state for shell and pairing effects (i.e.,  $\Delta=0$ ). The rest of the table lists the values for  $\Delta$ ,  $a$ , and  $\bar{E}_n$  which were computed from both Eqs. (6) and (7). The first line in the table for each nucleus gives the values for  $a$  and  $\bar{E}_n$  (for  $E_\gamma=E_m$ ) setting  $\Delta=0$ ; the second gives the best pair of values for  $\Delta$  and  $a$ , which were computed as described above. Note that although Eqs. (6) and (7) give widely different values for  $a$  (which differ by a factor of 2 or more), they yield remarkably consistent results for  $\Delta$ . Thus, unless this consistency is fortuitous, one can attach some validity to this determination of the influence of shell and pairing effects on the nuclear level density.

The values for  $\Delta$  thus derived are compared in Table X with the semiempirical values used by Fong<sup>27</sup> and Cameron<sup>28</sup> as shell and pairing corrections to the atomic mass formula. The present measurements, except for the case of Zr<sup>93</sup>, fall between the two sets of semiempirical values. The Zr<sup>91</sup> and especially the Zr<sup>93</sup> values suffer from the uncertainty in the extrapolation of the ring-ratio determination of  $\bar{E}_n$ . A systematic error in the ring-ratio calibration could have a large effect on the values derived for  $a$  and  $\Delta$ , but since this

would affect all the nuclei studied here in much the same way, the relative values for these parameters still would be nearly correct.

#### D. The Proposed Analog Giant Resonance

The problem of structure in the photon absorption cross section above the giant resonance has been the subject of much speculation. For instance, several

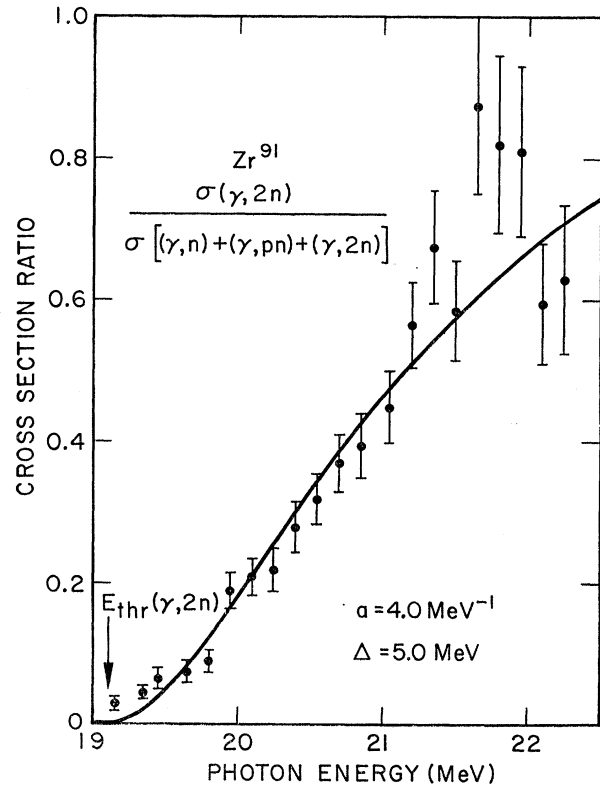


FIG. 14. Ratio of the  $(\gamma, 2n)$  cross section to the total photoneutron cross section for Zr<sup>91</sup>. The solid line is derived from the theoretical expression for the nuclear density of states given in Ref. 26, evaluated for a level density parameter  $a=4.0$  MeV<sup>-1</sup>, and including a shell-plus-pairing-effect parameter  $\Delta=5.0$  MeV, as explained in the text. The  $(\gamma, 2n)$  threshold value is taken from the data.

<sup>27</sup> P. Fong, Phys. Rev. **102**, 434 (1956).

<sup>28</sup> A. G. W. Cameron, Can. J. Phys. **35**, 1021 (1957).

TABLE IX. Nuclear level density parameters.

Nucleus	$\bar{E}_n$ (MeV) <sup>a</sup>	$U_{<}$ (MeV) <sup>b</sup>	$U_{>}$ (MeV) <sup>c</sup>	From Eq. (6) <sup>d</sup>			From Eq. (7) <sup>e</sup>		
				$\Delta$ (MeV)	$a$ (MeV <sup>-1</sup> )	$\bar{E}_n$ (MeV)	$\Delta$ (MeV)	$a$ (MeV <sup>-1</sup> )	$\bar{E}_n$ (MeV)
Y <sup>88</sup>	1.9	9.3	16.5	0	7.9	2.3	0	4.4	2.3
Zr <sup>89</sup>	1.7	9.0	11.1	1.0	7.4		1.2	3.7	
				0	5.4	2.4	0	2.5	2.5
Zr <sup>90</sup>	2.1	12.0	16.0	1.5	5.1		1.6	1.9	
				0	11.1	2.8	0	7.5	2.8
Zr <sup>91</sup>	2,2	7.2	12.2	4.8	8.1		5.0	4.0	
				0	11.8	2.3	0	7.1	2.5
Zr <sup>92</sup>	2.2 <sup>f</sup>	6.7	13.4	1.9	10.0		2.8	4.0	
				0	9.9	2.6	0	5.4	2.7
				3.1	7.6		3.9	1.6	

<sup>a</sup> From ring-ratio data.  
<sup>d</sup> Reference 25.

<sup>b</sup>  $U_{<} = E_{\text{thr}}(\gamma, 2n) - E_{\text{thr}}(\gamma, n)$ .  
<sup>c</sup> Reference 26.

<sup>e</sup>  $U_{>} = E_{\gamma\text{max}} - E_{\text{thr}}(\gamma, n)$ .  
<sup>f</sup> Upper limit of ring-ratio data; see text.

authors<sup>29-31</sup> have treated the question of photoprocesses induced by electric quadrupole radiation, but according to these theories, any quadrupole structure should occur above 26 MeV; the present data contain no evidence for such structure.

However, the suggestion recently has been made<sup>15,32,33</sup> that one might expect a second particle-hole state, akin to the giant-resonance state in the particle-hole model, but having an isobaric spin  $T_{>}$  one unit larger than the isobaric spin  $T_{<}$  of the ground- and giant-resonance states. This  $T_{>}$  state, according to Fallieros *et al.*,<sup>33</sup> should lie about 5 MeV above the giant resonance for Zr<sup>90</sup> and should have an oscillator strength equal to approximately 20% of the total dipole strength. Furthermore, neutron decay from such a state is inhibited although proton decay is not, since for neutron decay to a low-lying ( $T_{<} = \frac{1}{2}$ ) state of the residual nucleus, one would have  $\Delta T = \frac{3}{2}$  for the nuclear states, which cannot be taken up by the neutron. Therefore, such a neutron-decay process is forbidden by the iso-

baric spin selection rule. If it occurs, it is the result of the mixing of the  $T_{>}$  state into the many underlying  $T_{<}$  states in the compound system which, in turn, decay in the same way as the giant-resonance states.

As one can see from the total cross-section plots there is a clear upward excursion from the Lorentz lines in the cases of Y<sup>89</sup>, Zr<sup>90</sup>, and Zr<sup>91</sup>, all centered at about 21 MeV, and perhaps some sort of broader structure in Zr<sup>92</sup>, but this is not so clear. The evidence for any such structure in Zr<sup>94</sup> is doubtful. It is possible to identify these bumps with the "analog giant resonances" described in the previous paragraph. They lie about 4.5 MeV above the ordinary giant resonance and contain about 4 to 7% of the total photoneutron strength. The small contribution to the strength might be a consequence of the selection rule noted above. However, the  $(\gamma, p)$  cross section for natural zirconium<sup>21</sup> has a resonance shape centered at 22 MeV and has an integrated cross section about 2.5 times as large as these resonances in the photoneutron cross sections. Thus, if one also identifies this  $(\gamma, p)$  resonance with the analog giant resonance, one gets a total strength associated with it equal to about 16% of the total absorption cross section, in reasonable agreement with the prediction of Ref. 33. Moreover, it appears both from the Y<sup>89</sup> cross-section data, and especially from the Zr<sup>90</sup> cross-section and ring-ratio data, that the cross section in this energy region might contain structure.

## VI. SUMMARY

The photoneutron cross sections for Zr<sup>90</sup>, Zr<sup>91</sup>, Zr<sup>92</sup>, Zr<sup>94</sup>, and Y<sup>89</sup> were measured up to about 30 MeV. The average neutron energy as a function of photon energy also was determined. The masses of Y<sup>87</sup> and Zr<sup>88</sup> were determined from the  $(\gamma, 2n)$  thresholds of Y<sup>89</sup> and Zr<sup>90</sup>, respectively. The dominance of multiple neutron emission soon after this process becomes energetically possible agrees with the statistical nature of the decay mechanism, as well as the fact that photon absorption in the giant-resonance region is predominantly a compound-nucleus phenomenon. A Lorentz-shaped curve

TABLE X. Shell-plus-pairing-effect parameter  $\Delta$  (in MeV).

Nucleus	This experiment		Semiempirical values	
	From Eq. (6) <sup>a</sup>	From Eq. (7) <sup>b</sup>	Fong <sup>c</sup>	Cameron <sup>d</sup>
Y <sup>88</sup>	1.0 ± 0.3	1.2 ± 0.3	-1.2	2.2
Zr <sup>89</sup>	1.5 ± 0.2	1.6 ± 0.2	0	3.6
Zr <sup>90</sup>	4.8 ± 0.4	5.0 ± 0.4	3.2	5.7
Zr <sup>91</sup>	1.9 <sub>-1.9</sub> <sup>+0.6</sup>	2.8 <sub>-1.2</sub> <sup>+0.7</sup>	0	4.1
Zr <sup>92</sup>	3.1 <sub>-1.1</sub> <sup>+0.7</sup>	3.9 <sub>-0.7</sub> <sup>+0.5</sup>	0	2.8

<sup>a</sup> Reference 25.  
<sup>b</sup> Reference 26.

<sup>c</sup> Reference 27.  
<sup>d</sup> Reference 28.

<sup>29</sup> Y. K. Khoklov, Zh. Eksperim. i Teor. Fiz. **32**, 124 (1957) [English transl.: Soviet Phys.—JETP **5**, 88 (1957)].

<sup>30</sup> V. G. Shevchenko, N. P. Yudin, and B. A. Yur'ev, Zh. Eksperim. i Teor. Fiz. **45**, 180 (1963) [English transl.: Soviet Phys.—JETP **18**, 128 (1964)].

<sup>31</sup> M. Danos, W. Greiner, and B. C. Kohr, University of Freiburg Report, 1964 (unpublished).

<sup>32</sup> H. Morinaga, Z. Physik **188**, 182 (1965).

<sup>33</sup> S. Fallieros, B. Goulard, and R. H. Venter, Phys. Letters **19**, 398 (1965).

gives an accurate representation of the total photoneutron cross section near the peak of the giant resonance. From the collective models,  $\alpha$  and  $\beta$  are predicted to be constant. That this is so is evident in Table VII. The nuclear symmetry energies agree with those obtained from the semiempirical mass formula. The width of the giant resonance shows a marked increase as one proceeds away from the  $N=50$  closed neutron shell. The integrated photoneutron cross sections up to 30 MeV exhaust only 75 to 83%, and the areas under the corresponding Lorentz curves 87 to 96%, of the TRK sum-rule values even with no correction to the sum rule resulting from exchange forces. The second moment of the integrated cross section, which is proportional to the nuclear polarizability, obeys the sum-rule predictions; moreover, this quantity can be used to derive values for the nuclear symmetry energy which agree quite well with the values obtained from the hydrodynamic theory. In keeping with statistical theory, nuclear level density parameters were computed from the energy dependence of the ratio of the  $(\gamma, 2n)$  to the total photoneutron cross section and, combined with the

measurements of the average neutron energy at the peak of the giant resonance, were used to give a quantitative measure of the influence of shell and pairing effects on the nuclear density of states. There are indications of a second, weaker giant resonance lying somewhat higher in energy and perhaps related to photon excitation of a state or states of isobaric spin one unit higher than that of the ground state of the target nucleus. It is hoped that the variation of all the above quantities with proton and neutron number near the  $N=50$  closed shell as determined in this study might throw light on the theories of shell effects in the nucleus.

#### ACKNOWLEDGMENTS

The authors wish to thank R. Knox for help in taking the data, Dr. H. S. Davis for assistance in the data analysis, Miss C. Hunt for computer programming, and E. Dante and the operating and maintenance staff of the accelerator. The authors also profited from discussion with Dr. A. Kerman, Dr. M. Weiss, and Dr. F. H. Lewis.